Wind and Structures, *Vol. 22, No. 1 (2016) 65-87*
DOI: http://dx.doi.org/10.12989/was.2016.22.1.065

Capacity of a transmission tower under downburst wind loading

T.G. Mara*[1], H.P. Hong[2], C.S. Lee[2,3] and T.C.E. Ho[1]

[1]*The Boundary Layer Wind Tunnel Laboratory, University of Western Ontario, London, ON, Canada, N6A 5B9*
[2]*Department of Civil and Environmental Engineering, University of Western Ontario, London, ON, Canada, N6A 5B9*
[3]*Rowan Williams Davies & Irwin Inc., 650 Woodlawn Road West, Guelph, ON, Canada, N1K 1B8*

(Received December 13, 2014, Revised September 25, 2015, Accepted October 22, 2015)

Abstract. The wind velocity profile over the height of a structure in high intensity wind (HIW) events, such as downbursts, differs from that associated with atmospheric boundary layer (ABL) winds. Current design codes for lattice transmission structures contain only limited advice on the treatment of HIW effects, and structural design is carried out using wind load profiles and response factors derived for ABL winds. The present study assesses the load-deformation curve (capacity curve) of a transmission tower under modeled downburst wind loading, and compares it with that obtained for an ABL wind loading profile. The analysis considers nonlinear inelastic response under simulated downburst wind fields. The capacity curve is represented using the relationship between the base shear and the maximum tip displacement. The results indicate that the capacity curve remains relatively consistent between different downburst scenarios and an ABL loading profile. The use of the capacity curve avoids the difficulty associated with defining a reference wind speed and corresponding wind profile that are adequate and applicable for downburst and ABL winds, thereby allowing a direct comparison of response under synoptic and downburst events. Uncertainty propagation analysis is carried out to evaluate the tower capacity by considering the uncertainty in material properties and geometric variables. The results indicated the coefficient of variation of the tower capacity is small compared to those associated with extreme wind speeds.

Keywords: transmission towers; downbursts; extreme winds; nonlinear analysis; Monte Carlo technique

1. Introduction

Transmission structures serve a vital purpose in society as components of electrical transmission networks. Electrical transmission networks span great distances while providing the end user with electricity. Transmission structures may experience strong synoptic wind events (e.g., winter storms) or localized high intensity wind events (HIW) events such as thunderstorm gust fronts, downbursts or tornadoes. Wind loads on structures resulting from synoptic events are considered to be characterized by a traditional atmospheric boundary layer (ABL) wind speed profile, while HIWs are characterized by transient wind speed profiles which vary between events. Though different in both meteorological and loading characteristics, each type of wind has been found to result in structural damage and failure. A well-documented example was the failure of 19

*Corresponding author, Research Engineer, E-mail: tmara3@uwo.ca

http://www.techno-press.org/?journal=was&subpage=8 ISSN: 1226-6116 (Print), 1598-6225 (Online)

towers due to multiple downburst events in the southern portion of the Manitoba Hydro power transmission corridor (McCarthy and Melsness 1996). The social and economic fallout of this event served as the impetus to better understand the characteristics of HIWs (Hangan *et al*. 2008, Banik *et al*. 2008), their loadings (Mara *et al*. 2010, Lin *et al*. 2012), and the response of transmission structures to HIWs (Shehata *et al*. 2005, Shehata and El Damatty 2008, Banik *et al*. 2010).

The term 'downburst' was coined by Fujita (1976) to describe a strong convective downdraft which impinges on the surface of the earth, resulting in an outflow of strong winds close to ground level. Downbursts are further classified into macrobursts (outflow winds extending to distances greater than 4 km) and microbursts (outflow winds limited to distances of 4 km or less). Time histories of wind speed and direction of a microburst were recorded at Andrews Air Force Base (AAFB) on 1 August 1983; the record shows a peak wind speed of approximately 67 m/s (notated as 130+ kts) on the front side of the outflow at a height of 4.9 m (Fujita 1985). This was the most intense downburst outflow observed during the NIMROD and JAWS projects (described in Fujita (1985)), although it is expected that the probability of occurrence of microbursts of this magnitude is low. Two HIW events similar to a downburst, a derecho and rear flank downdraft (RFD), were observed during the Texas Tech Thunderstorm Outflow Experiment (TTTOE) (Orwig and Schroeder 2007). The records from this event include mean velocity profiles, turbulence intensity profiles, and information useful for the integral length scales and spatial correlation of the outflow. Spectral and correlation characteristics of the RFD were discussed by Holmes *et al*. (2008) with regards to the span reduction factor for transmission line design.

While the field studies by Fujita shed light on downburst occurrence and damage capability, and the measurements of the TTTOE provided valuable wind profile characteristics, instances of full-scale downburst observation and measurement remain quite rare. As a result, the majority of work in the structural engineering community has proceeded adopting a numerical approach to downburst wind fields, while using the few full-scale examples as references for model validation. Holmes and Oliver (2000) developed an empirical model of a downburst based on an impinging jet for the simulation of damage footprints. The impinging jet approach was also used by Wood *et al*. (2001) to investigate the downburst wind speed profiles over various topography; they found the maximum horizontal velocity to occur at a distance of approximately 1.5 jet diameters from the center of impingement. Savory *et al*. (2001) modelled the time history of a translating microburst using an impinging jet combined with a previously developed wind velocity profile in order to apply transient loading to a transmission tower. It was found that the displacement of the tip of the tower was proportional to the applied wind loading throughout the duration of the microburst passage, which implies the response is quasi-static. A transient downburst wind field was modelled using a stationary axisymmetric impinging jet by Hangan *et al*. (2003), which provided a spatio-temporal flow model that could be applied to structures. Kim and Hangan (2007) compared the time series of the wind speed in the simulated outflow to the full-scale measurements obtained in the TTTOE, showing good agreement. The downburst wind fields generated in the Hangan *et al*. (2003) simulation were applied to a structural model in the study described in this paper. This downburst wind field model was selected due to its capability to model the primary and secondary vortex rings, which is necessary to adequately characterize the shape of the downburst wind speed time history. It is important to note that unlike ABL wind, where a fixed wind speed profile with height is assumed, the wind speed profile in a downburst outflow is transient. In addition to varying in time, the profile is a function of the size and strength of the downburst, as well as the distance between the downburst center (point of touchdown) to the point of interest. This makes a

meaningful definition of a reference wind speed, or maximum wind speed, resulting from a particular downburst challenging. This has implications for the development and application of design codes. Therefore, a solution to this problem through simplification of design verification for structures is worth exploring.

Few studies directed at the assessment of structural response to downburst winds are available in the literature. An analysis of a transmission tower-line system having guyed towers under simulated downburst wind was carried out by Shehata *et al*. (2005). In the analysis, the forces on the conductors and ground wires were calculated using geometric nonlinear analysis, and were applied in combination with quasi-static wind loads on the tower. The use of quasi-static wind forces on the tower was justified based on a frequency comparison showing that the fundamental frequency of vibration of the tower is much higher than the predominant frequency content of the downburst (without the fluctuating component), thereby making the resonant component negligible. The use of quasi-static analysis for a similar tower analysis was also applied by Darwish and El Damatty (2011). This approach is consistent with the approach taken for the treatment of gust factors for transmission towers widely used in industry (e.g. ASCE 2010).

Based on the application of the nonlinear incremental dynamic analysis (IDA) and nonlinear static pushover (NSP) methods to wind loads on a 2-D numerical model of a self-supported transmission tower, Banik *et al*. (2010) observed that the capacity curve, as defined in terms of the total horizontal force (analogous to the total reacting base shear force if inertial forces are negligible) versus the tip displacement, can be adequately assessed using the NSP method. Furthermore, it was found that the capacity of the tower at the incipient yield and collapse is influence by the wind speed profile over the height of the tower. As the failure and reliability of a tower depend directly on its capacity curve, the evaluation of these quantities under downburst loading is relevant and important for both the design of new towers and the evaluation of existing towers.

The present study is focused on the parametric investigation of the capacity curve of a self-supported transmission tower under multiple scenarios of downburst wind loading, which provides the yield and maximum capacity (i.e., capacity at the incipient collapse). Evaluation of the difference between the tower capacity curve under ABL and modeled downburst wind is made, as well as an assessment of the effect of uncertainty in material properties. For the analysis, wind load in the longitudinal and transverse directions to the transmission tower line system are considered. The goal of the research is to develop a simple practical solution which can be directly used to evaluate the performance of a tower under downburst wind loading. Both material and geometric nonlinearity are considered in the analysis of the 3-D transmission tower model.

2. Modelling of the transmission tower, ABL wind loads and effects

2.1 Numerical model of the transmission tower

A self-supported lattice transmission tower design was provided by Manitoba Hydro and modeled in ANSYS Multiphysics 9.0 (ANSYS 2007). The design of the prototype tower considered wind, ice and other loading conditions. The tower members are modeled using 2-node beam elements having 6 degrees of freedom at each node; these are BEAM188 elements specified to have an L-section corresponding to the prototype geometry. This element was selected for its suitability for modeling slender beam-like structures and its performance in nonlinear large-strain

applications. All multi-bolted moment-resisting connections are assumed to be rigid. The masses of the conductors and ground wire are applied as lumped masses to the structure at the corresponding nodes. A 3-D view of the numerical model of the tower is shown in Fig. 1.

The numerical model of the tower includes the effects of material nonlinearity, which are based on the material properties of the structural steel and the built-in bilinear isotropic (BISO) hardening constants in ANSYS. The behaviour of the material under deformation corresponds to a bilinear stress-strain curve where the slope in the elastic range is taken as the modulus of elasticity of the structural steel, while the slope in the post-yield range is defined by the tangent modulus. The section properties of the structural members of the tower and wires, along with the nominal dimensions of the structural steel and distribution by panel, are shown in Table 1. Geometric nonlinearity was also considered through the use of a large-deformation analysis, which was necessary due to the deflections expected at the tip of the tower. This is implemented in ANSYS through activation of a large-strain analysis, which if required, accounts for changes in the stiffness matrix that result from the deformed shape or orientation of an element at each equilibrium iteration. Each of the analysis techniques described in the following sections employed both material and geometric nonlinearity. A force-based criterion was used for convergence. A total of 959 elements and 405 nodes are used in the modeling of the tower. Additional details on the finite element model are provided in Mara and Hong (2013).

2.2 Loads under synoptic wind

Wind loads on structures resulting from synoptic events are considered to be characterized by a traditional ABL (i.e., power law) wind speed profile. Design wind loads for transmission towers are specified in CAN/CSA C22.3 No. 60826-10 (referred to herein as CSA-2010) (CAN/CSA 2010), as well as ASCE Manual No. 74 (referred to herein as ASCE-74) (ASCE 2010). CSA-210 adopts the International Electrotechnical Commission (IEC) Standard 60826:2003 for design criteria of overhead transmission lines (IEC 2003), which is used throughout the world for the design of transmission systems.

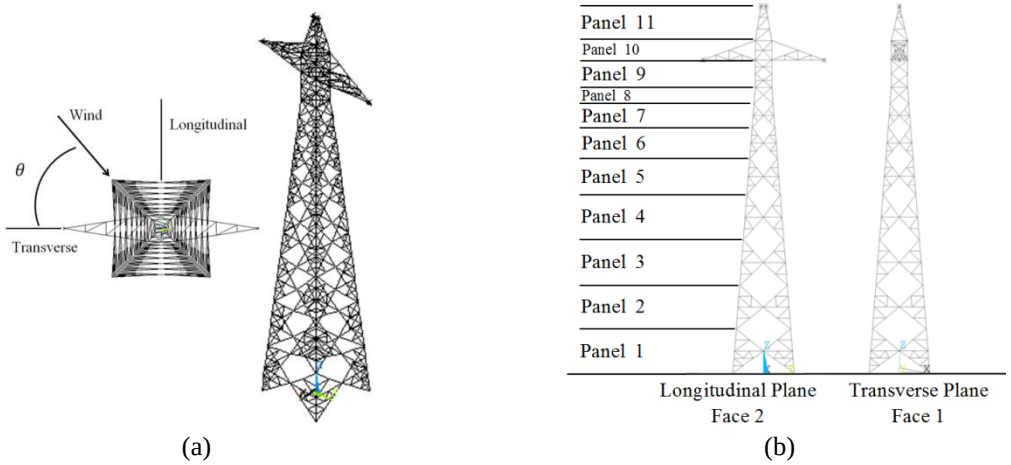

(a) (b)

Fig. 1 Transmission tower (the conductors are located at the end of the arms and the ground wire is located near the tip of tower): (a) 3-dimensional view and(b) definition of loading panels according to code-based design procedure

As the current analysis is carried out on a structure designed and built in Canada, it is prudent to invoke the specifications in CSA-2010 for later comparison. For the calculation of the wind loads, the prototype tower was divided into 11 representative sections, referred to as panels, along its height as shown in Fig. 1. An exposure representative of open country terrain was used, which corresponds to a roughness length of 0.03 m and power law coefficient of 0.16. It should be noted that the reference wind speed in CSA-2010 is based on a 10-minute mean wind speed at a height of 10 m in open country terrain; the implications of this on the results obtained through numerical analysis will be discussed later. It is assumed that the background component of the dynamic response is dominant, and that the resonant component can be neglected. This approach is taken for typical transmission towers in CSA-2010 and ASCE-74, and is based on the consideration of structural properties of the transmission tower and the characteristics of the wind (see Davenport 1979).

In accordance with CSA-2010, the wind loads on a single panel are calculated by

$$A_t = 0.5\tau\mu V_R^2 G_t (1 + 0.2\sin^2(2\theta)) (S_{t1}C_{xt1}\cos^2\theta + S_{t2}C_{xt2}\sin^2\theta) \quad (1)$$

where A_t (N) is the total wind loading on the panel in the direction of the wind; τ is an air density correction factor taken to be 1; μ is the density of air taken to be 1.225 kg/m^3; V_R (m/s) is the reference wind speed based on a 10-minute mean wind speed at 10 m height in open country terrain; θ is the angle of attack (yaw angle) illustrated in Fig. 1; S_{ti} (m^2) is the total surface area projected normally on the corresponding i-th face, i = 1 and 2 (see Fig. 1); C_{xti} is the drag coefficient for the corresponding i-th face; and G_t is a combined wind factor accounting for roughness of terrain and height of the panel. In this case, faces 1 and 2 correspond to the transverse and longitudinal faces of the tower, respectively.

The wind loads on the conductors and ground wire are calculated by

$$A_c = 0.5\tau\mu V_R^2 G_c G_L d L C_{xc} \sin^2\Omega \quad (2)$$

where A_c (N) is the total load on the line; C_{xc} is the drag coefficient of the line taken to be 1.0; G_c is the combined wind factor for the line; G_L is the span factor based on the length of the span; d (m) is the diameter of the wire; L (m) is the wind span of the wires; and Ω is the angle of attack (yaw angle) between the wind direction and the wires. If there is no line angle between consecutive towers, Ω equals (90 - θ).

The values of each parameter for each of the panels and wires are listed in Table 2, along with the calculation of the wind load on each panel, wire and overall structure. For the calculation, the height-dependent values of G_t and G_c required for Eqs. (1) and (2) are directly obtained from the equations supplied in CSA-2010. It is shown that the total wind load in the longitudinal and transverse directions are $128.8V_R^2$ N and 220.4 V_R^2 N, respectively. The load in the transverse direction is much greater due to the contributions of the conductors and ground wire.

2.3 Capacity curves for ABL and rectangular wind loading

The nonlinear static pushover (NSP) analysis method is a commonly used technique to evaluate the capacity of a structure under earthquake loading (e.g., Krawinkler and Seneviratna 1998). More recently, the NSP method has been applied to steel lattice towers considering point loading representative of prototype pushover tests (Lee and McClure 2007), wind loading for transmission towers (Banik *et al*. 2010) and wood-frame structures (Lee and Rosowsky 2006), and roof panel

uplift under wind load (He and Hong 2012). The procedure is used to evaluate the nonlinear force-deformation relationship and identify the yield and maximum capacity of a structure by monotonically increasing the applied forces while maintaining a constant loading profile. In the NSP analysis, the resulting displacement is calculated for each incremental increase in applied force. The resulting force-deformation coordinates define a capacity curve, which describes the nonlinear force-deformation relationship of the structure. A capacity curve showing the behaviour of a nonlinear inelastic system is shown in Fig. 2. For the current analysis, the force represents the total applied horizontal wind load (which is equivalent to the resultant base shear), while the deformation represents the displacement of the tip of the tower. The curve is approximated by a bilinear system; the yield capacity of the system is defined by the point of intersection of the elastic and post-yield tangents (as shown in Fig. 2), while the maximum capacity is defined by the incipient collapse of the tower. Note that Banik *et al*. (2010) showed that the capacity curve obtained using the NSP method provides a good approximation to that obtained from nonlinear incremental dynamic analysis, and that the curves determined in such a manner represent the effect of a peak wind load on the tower. The estimated capacity can therefore be viewed as representative of response under a short-duration gust. This consideration and analysis procedure is also applied in the following analysis.

To establish a basis for comparison of capacity curves resulting from wind profiles representative of downburst outflow wind, the capacity curves for two basic wind profiles were first examined. For this, the mean values of the structural material properties and geometric variables were employed, and the effect of their uncertainty was neglected. The first wind profile represents a traditional ABL wind profile based on the power law in open country terrain (power law exponent of α). Assuming that the wind speed is fully correlated spatially, or coherent (for this or any other wind profile considered in this study), the adopted power law suggests that the 3-second gust mean wind speed at a height z (m) above the ground, $V_{3s}(z)$, is given by

$$V_{3s}(z) = (z/10)^{\alpha} V_{3s,10m} \tag{3}$$

where $V_{3s,10m}$ represents the 3-second gust mean wind speed at a height of 10 m. A value of α equal to (1/9.5) is suggested in ASCE-74 for a 3-second gust mean wind speed profile in open country terrain, while a value of 0.16 is specified by CSA-2010 for the 10-minute mean wind speed profile.

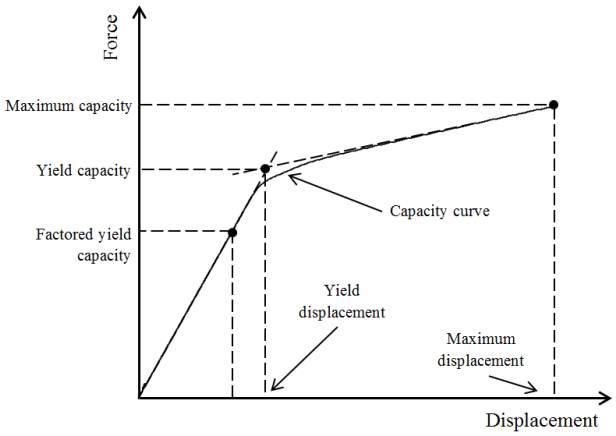

Fig. 2 Force-deformation or capacity curve for an inelastic system

The latter results in a greater increase in wind speed over the height of a structure than the former. As it will be shown, the consideration of the ABL wind profile is directed at developing a lower bound for the capacity curve of the tower, and a larger value of α leads to a lower capacity curve. A power law coefficient of α = 0.16 was therefore applied in the remaining part of the study, which results in a slightly conservative estimate of the lower bound of the capacity curve if gust mean wind speed averaging times are considered.

The second profile is rectangular in shape, which represents a uniform wind profile over the height of the tower (i.e., $V_{3s}(z) = V_{3s,10m}$ over the height). This profile is selected, as it will be shown, since it resembles the downburst wind profile for the range of parameters considered in this study over the height range of interest (5 to 50 m above the ground). Additional discussions on the effect of different wind profiles on structures can be found in Banik *et al*. (2010), Mara and Hong (2013), and Lombardo *et al*. (2014).

The NSP analysis was carried out for the ABL and rectangular wind profiles and is summarized in the following steps:

1. The wind speed at the height of each structural connection (represented as nodes in the numerical model) is calculated based on the wind speed of the selected loading profile (ABL or rectangular).

2. The wind load for each panel is calculated based on the wind speed found in Step 1, and corresponding geometric and aerodynamic parameters of the panel of interest. Note that while aerodynamic properties are only considered for 11 unique panels, the wind speed is calculated at 45 locations (corresponding to the node heights in the numerical model shown in Fig. 1) along the height of the tower to account for intra-panel variation in wind speed.

3. The total wind load calculated for each panel is distributed evenly among the nodes in the panel. The wind loads on the conductors and ground wire are calculated according to Eq. (2) and transferred to the tower as point loads at the nodes corresponding to the wire-structure connections.

4. Beginning at a very low wind speed, the wind load is applied to the numerical tower model in ANSYS and convergence is achieved. The output includes the total base shear and the displacement of the tip of the tower, which are compiled in the capacity curve.

5. Provided Step 4 converged, the wind speed is increased by a small increment and Steps 1 through 4 are repeated. If the model fails to converge, the analysis is terminated and collapse of the tower has occurred.

The wind loads on the conductors and ground wires are based on half the wind span of the lines of each side of the tower, resulting in a total loading span for each wire of 488 m (2 x 244 m). The values used for the tower dimensions and aerodynamic coefficients of each panel are included in Table 1.

Based on the above considerations, the wind load on each panel along the height of the tower in terms of $V_{3s,10m}$ were calculated and are shown in Table 3. As the variation of wind speed over height is considered using $V_{3s}(z)$, and that the wind speeds are gust wind speeds, G_t and G_c in Eqs. (1) and (2) were set equal to 1.0. Note that the wind load in CSA-2010 is based on a 10-minute mean wind speed at 10 m height, $V_{10min,10m}$, and those shown in Table 3 were estimated in terms of $V_{3s,10m}$. In addition, a more detailed description of the wind loading profile was utilized in the analysis compared to the piecewise approach applied when using CSA-2010. To facilitate the discussion of the tower capacity in the context of codified design, the capacity in terms of $V_{3s,10m}$ were converted to terms of $V_{10min,10m}$. For the conversion, the ratio $V_{3s,10m}/V_{10min,10m}$ = 1.43 for open country terrain (Durst 1960) was used. The wind loads are then $145.8V^2_{10min,10m}$ for the longitudinal

direction and $286.3V^2_{10min,10m}$ for the transverse direction. Comparison of these values to those shown in Table 2 indicates that the use of the previously described procedure leads to 11% greater wind load (i.e., 5.7% greater wind speed) in the longitudinal direction and 23% greater wind load (i.e., 12.3% greater wind speed) in the transverse direction. The differences are attributed to the use of the ABL profile and more detailed wind load variation over the height in the above procedure, compared to the use of G_t and the approach in CSA-2010. In all cases, the detailed analysis and considered ABL profile lead to a more conservative estimated wind load.

Table 1a Nominal section properties of the structural members of the tower and wires

	Units (m)		
	Angle	Thickness	Member Key
Chords and Horizontals	0.0445 x .0445	0.00318	a
	0.0445 x .0445	0.00953	b
	0.0508 x 0.0508	0.00318	c
	0.0508 x 0.0508	0.00476	d
	0.0635 x 0.0635	0.00476	e
	0.0762 x 0.0762	0.00476	f
Diagonals and Legs	0.0762 x 0.0762	0.00635	D1
	0.0889 x 0.0635	0.00635	D2
	0.0889 x 0.0889	0.00635	D3
	0.1016 x 0.1016	0.00476	D4
	0.127 x 0.127	0.00794	L1
	0.127 x 0.127	0.00953	L2

Table 1b Structural steel distribution by panel

	Members in Resisting Direction		Support
Panel	Longitudinal	Transverse	Plan
1	L2, D2, a, c, d	L2, D1, a, c, d	
2	L2, D2, a, b, d	L2, D2, a, b, d	
3	L2, D3, c, e	L2, D2, c, e	
4	L2, D3, a, e	L2, D2, a, e	
5	L1, D3, a, d	L1, D2, a, d	
6	L1, D3, a, b	L1, D2, a, b	
7	L1, D3, a, c	L1, D3, a, c	
8	L1, D4, d	L1, D3, d	
9	D3	D3, a	a
10	D3, e	D3, D4, a, d, f	L1, D1, a, b, d, e
11	a, e	D1, a, b, c	

Table 1c Nominal section properties of the conductors

Property	Conductor	Ground wire
Diameter (m)	0.0381	0.0184
Density (kg/m)	2.354	1.046
Modulus of Elasticity (GPa)	58.6	125.3
Design Span (m)	488	488

Table 1d Properties and uncertainty associated with structural steel

Random Variable	Mean	COV	Distribution Type
Density	7.8 kg/m^3	0.05	Lognormal
Modulus of elasticity	2E+8 kN/m^2	0.1	Lognormal
Ratio of post-yield stiffness to initial stiffness	0.05	0.1	Lognormal
Section dimensions	Varies with section[1]	0.025	Lognormal
Yield strength	3.3E+5 kN/m^2	0.1	Lognormal

Note: The mean of section dimension is considered to be equal to nominal section dimension shown in Table 1(a)

Table 2a Nominal wind load calculated using CSA-2010 for the tower shown in Fig. 1.

		Longitudinal direction				Transverse direction			
Panel	Height (m)	Area (m^2)	C_d	G_t	F$_d$ (N)/V^2_R	Area (m^2)	C_d	G_t	F$_d$ (N)/V^2_R
1	2.8	4.51	3.39	1.76	16.48	4.51	3.39	1.76	16.48
2	8.5	3.88	3.42	1.9	15.44	3.88	3.42	1.9	15.44
3	14.3	3.74	3.36	2.03	15.62	3.74	3.36	2.03	15.62
4	20.1	3.46	3.29	2.15	14.99	3.46	3.29	2.15	14.99
5	25.3	2.75	3.16	2.25	11.98	2.75	3.16	2.25	11.98
6	29.6	2.27	3.05	2.32	9.84	2.27	3.05	2.32	9.84
7	33.1	1.76	2.85	2.37	7.28	1.76	2.85	2.37	7.28
8	35.65	1.1	2.8	2.4	4.53	1.1	2.8	2.4	4.53
9	38.45	1.7	2.8	2.44	7.11	1.52	2.91	2.44	6.61
10	41.45	4.73	2.89	2.47	20.68	0.89	3.08	2.47	4.15
11	44.9	1.17	2.71	2.51	4.87	1.17	2.71	2.51	4.87
			Longitudinal		128.83 V^2_R		Transverse		111.79 V^2_R

Table 2b Nominal wind load calculated using CSA-2010 for the conductor

Cable	Height (m)	d (m)	L (m)	C_d	Number	G_L	G_w	F_d (N)/V^2_R
Conductor	35.65	0.076	488	1	2	0.919	2.31	96.44
Ground wire	44.9	0.0184	488	1	1	0.919	2.4	12.13
					Transverse (wires)			108.60 V^2_R
					Transverse including those on tower (total)			220.39 V^2_R

The NSP method is carried out for the ABL and rectangular wind profiles, and the obtained capacity curves are shown in Figs. 3(a) and 3(b) for the longitudinal and transverse directions, respectively. For the longitudinal or transverse loading cases, the total applied horizontal force and tip displacement are in plane with the applied load. Fig. 3(a) shows that the yield capacities of the tower in the longitudinal direction are 515.3 kN and 559.4 kN for the ABL and rectangular wind profiles, respectively. The capacity of the tower at incipient yield for the rectangular wind profile is greater than those for the ABL wind profile. However, this trend is reversed if the incipient collapse is considered, and a large horizontal deformation is associated with the ABL profile. In this case, the capacities at incipient collapse, or the maximum capacity, of the tower in the longitudinal direction are approximately 665.6 kN and 637.8 kN for the ABL and rectangular wind profiles, respectively. Using the calculated wind load shown in Table 3, and the estimated capacity at incipient yield or collapse, the corresponding $V_{3s,10m}$ values are calculated and also shown in the table. The values indicate that the tower can sustain a $V_{3s,10m}$ = 85 m/s without yield in the longitudinal direction if the ABL profile is considered, or $V_{3s,10m}$ = 97.5 m/s if the rectangular profile is considered. Similar magnitude of difference between the critical wind speed for incipient collapse can also be observed from Table 3; this difference illustrates the potential influence of the shape of the wind profile on the estimated capacity of the tower.

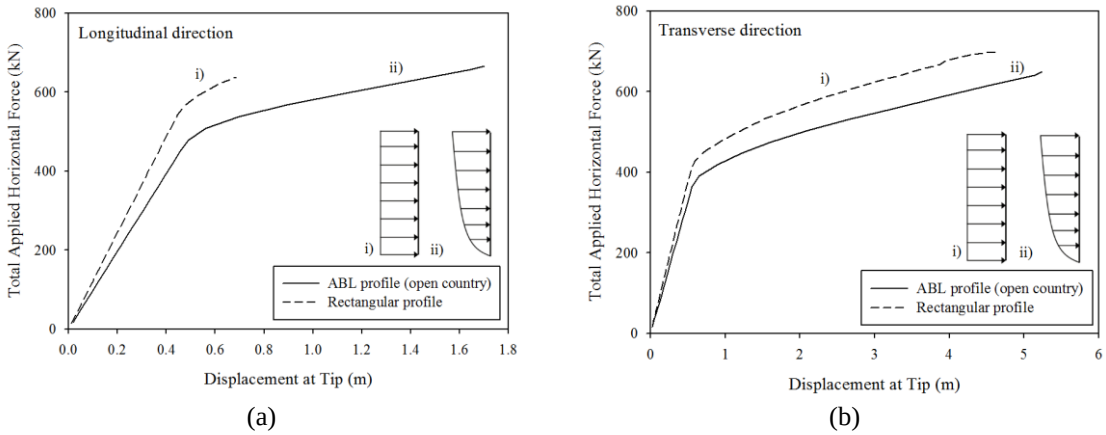

(a) (b)

Fig. 3 Capacity curves for ABL and rectangular wind distributions in (a) longitudinal direction and (b) transverse direction

Comparison of the results in Figs. 3(a) and 3(b) indicates that the yield capacities of the tower in the transverse direction are significantly lower than those in the longitudinal direction, although the capacities at incipient collapse in the transverse direction are comparable to those in the longitudinal direction. The tower can withstand a greater (total) horizontal wind load under the rectangular wind load distribution due to the lower load contributions of: i) the cross-arm of the tower in the longitudinal direction; and, ii) the wires in the transverse direction. However, it is shown that if the ABL profile is applied, more deformation occurs in the post-yield range. This is again attributed to the load concentration in the upper portion of the tower. The estimated capacity at incipient of yield and collapse for the transverse direction, as well as their corresponding $V_{3s,10m}$ wind speeds, are summarized in Table 3. It is indicated that the critical wind speed that the tower can withstand is governed by the capacity and critical wind speed associated with the transverse direction. In all cases, the critical values in terms of $V_{10min,10m}$ are also calculated (using $V_{3s,10m}/V_{10min,10m} = 1.43$) and shown in the table.

This implies that at the incipient yield, the critical $V_{10\text{-min},10\text{m}}$ equals 39.1 m/s (i.e., 141.5 km/hr), a wind speed that is greater than the (factored) design wind speed for many locations suggested in CAN/CSA-C22.3 (CSA 2010). This implies that the design of tower is not governed by wind alone. Note that the inferred critical wind speed does not include the uncertainty in the material properties for the designed tower. This is to be discussed in the next section.

2.4 Uncertainty propagation analysis and discussion

The geometric and material variables of structures are uncertain; this uncertainty influences the calibration of load and resistance factors in the codification process (Ellingwood *et al*. 1980, Bartlett *et al*. 2003). To assess the effects of these uncertainties on the tower capacity under ABL wind loading, the simple Monte Carlo technique is used to sample the values of material properties and geometric variables from their probability distribution models (shown in Table 1).

Table 3 Yield and maximum capacities and corresponding wind speed for the tower in the longitudinal and transverse directions

	ABL profile		Rectangular	
	Longitudinal	Transverse	Longitudinal	Transverse
Wind load (N) in terms of	$71.3V^2_{3s,10m}$	$140\ V^2_{3s,10m}$	$58.9V^2_{3s,10m}$	$102.9V^2_{3s,10m}$
$V^2_{3s,10m}$ and of ($V^2_{10\text{-min},10m}$)	($145.8V^2_{10\text{-min},10m}$)	($286.3V^2_{10\text{-min},10m}$)	($120.4V^2_{10\text{-min},10m}$)	($210.9V^2_{10\text{-min},10m}$)
Yield capacity (kN)	515.3	442.5	559.4	487.7
Maximum capacity (kN)	665.6	649.8	637.8	699.9
Critical $V_{3s,10m}$ ($V_{10\text{-min},10m}$) for	85	56.2	97.5	68.8
yield (m/s)	(59.4)	(39.3)	(68.2)	(48.1)
Critical $V_{3s,10m}$ ($V_{10\text{-min},10m}$) for	96.6	68.1	104.1	82.5
collapse (m/s)	(67.6)	(47.6)	(72.8)	(57.7)

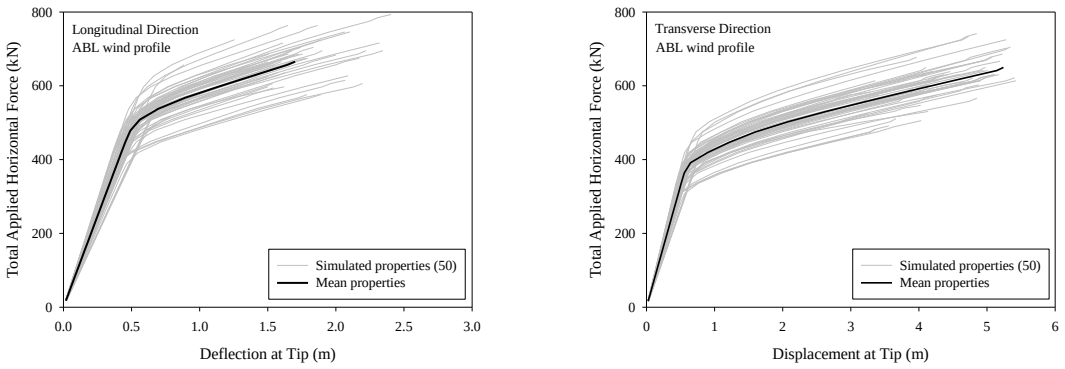

Fig. 4 Capacity curves resulting from uncertainty analysis (50 simulations) for the structural properties of the tower for ABL wind distribution in the (a) longitudinal direction and (b) transverse direction

Capacity curves of the tower for simulated sets of structural and geometric properties were developed; the properties sampled for each element were held consistent within each simulated tower. The adopted probabilistic models shown in Table 1 are based on those provided by Manitoba Hydro, as well as those found in the literature and used for code calibration (Ellingwood *et al*. 1980, Bartlett *et al*. 2003, Haukaas and Der Kiureghian 2006). Based on the ABL wind profile, 50 samples of capacity curves are obtained and shown in Figs. 4(a) and 4(b) for wind loading in the longitudinal and transverse directions, respectively. The mean and coefficient of variation (cov) of the yield and maximum tower capacities from these samples were calculated and shown in Table 4. In all cases, the estimated cov values are within 0.083 and 0.096. This range of cov is slightly lower than the highest cov values of 0.10 considered for material properties, while much less than the cov encountered for extreme wind load effects (i.e., Bartlett *et al*. 2003) of about 0.25 to 0.4.

Since the cov of the annual maximum wind speed is about 0.138 for Canada (Hong *et al*. 2014) and the cov of the wind load is at least twice of this value, the cov of the capacity curve is relatively small as compared to that of the wind load effect. However, for a given wind speed, the cov of the capacity curve affects the calculated probability of failure. In fact, if the maximum capacity is assumed to be normally distributed, its 0.01-fractile for transverse loading equals 482.2 kN (i.e., = 618.5×(1-2.32×0.096)). This translates to a critical wind speed $V_{3s,10m}$ equal to 58.7 m/s, resulting a 16% reduction in the critical wind speed (as compared to 68.1 m/s shown in Table 3). In other words, if $V_{3s,10m}$ equal to 58.7 m/s (i.e., $V_{10\text{-}min,10m}$ = 41.0 m/s) is applied to 100 towers, one of the towers will collapse (i.e., failure probability equals 1%). The small failure probability for this strong wind indicates that the design of the considered tower is likely to be governed by loads other than the wind load alone (e.g., the design may be governed by the combination of ice and wind loads).

It must be emphasized the use of such a tower in the present study is adequate since it does not affect the conclusions that can be drawn from the relative differences between the capacity curves obtained using different analysis method. However, the estimated critical wind speeds are only applicable to this considered tower. Since the estimation of tower reliability and design code

calibration which are important are outside of the scope of the present study, no further analysis of the uncertainty of the capacity curve was carried out in the remainder of this study.

3. Downburst wind loads

3.1 Application of a numerical stationary downburst simulation

The strong winds in a downburst outflow are the result of a cool air mass descending from the upper atmosphere coming into contact with the surface of the earth. This phenomenon results in a rolling vortex which translates outward from the center of the downburst (described as the point of touchdown), characterized by a gust front with strong winds over the height range of most engineered structures. Spatio-temporally varying wind fields from a simulation of a stationary downburst event (Hangan *et al*. 2003) were obtained and processed. As the downburst simulation was carried out parametrically, the simulation and output were first converted to full-scale dimensions based on values describing the size and strength of the event. Fig. 5 illustrates the size denoted by jet diameter, D_{jet}, and the strength denoted by the jet velocity, V_{jet}, and the distance from the center of the downburst to a point of interest, r. The horizontal wind speed in the downburst outflow profile is provided from the simulation as a ratio to V_{jet}, and is notated as V_{hor}. The simulation time scale, t_s, representing the time step used in the downburst simulation, differs from the time scale t at full-scale; the conversion from t_s to t depends on the values of V_{jet} and D_{jet} (Hangan *et al*. 2003). A ratio, r/D_{jet}, is used for parametric investigation of downburst effects among different sizes of downbursts, rather than using a specific value of r, as the use of a specific value would not incorporate scaling with D_{jet}. Further description of the numerical downburst simulation can be found in Kim and Hangan (2007).

Table 4 Statistics of tower capacity under longitudinal and transversal loading (based on 50 simulations).

	Yield capacity (kN)		Maximum capacity (kN)	
Direction	Mean	cov	Mean	cov
Longitudinal	508.3	0.094	664.5	0.083
Transverse	436.2	0.096	618.5	0.095

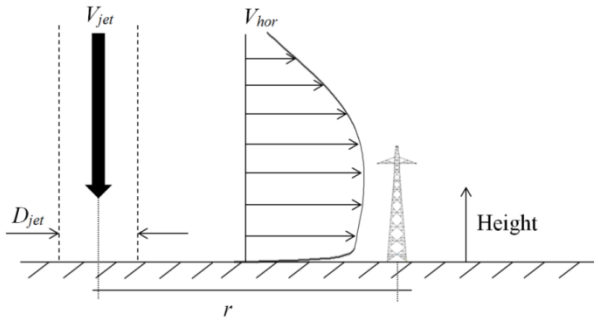

Fig. 5 Elevation plot showing the parameters in the numerical downburst simulation (downburst outflow scale to r/D_{jet} = 1.3, D_{jet} = 500 m)

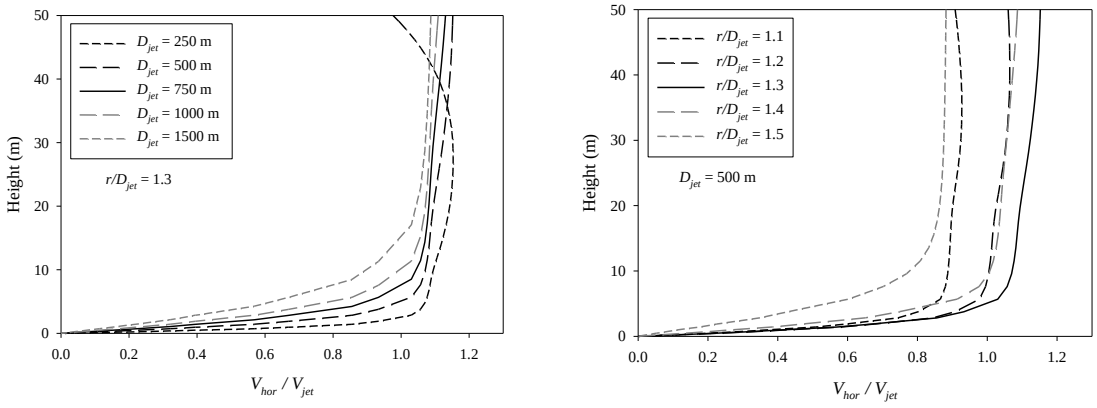

Fig. 6 Variation of horizontal velocity wind profiles with downburst parameters (a) D_{jet}, and (b) r/D_{jet}

The use of a maximum wind speed at a reference height to describe the strength of a downburst event presents a difficulty in interpretation, as the shape of the wind speed profile with height varies with time, the size of the downburst, and the distance from downburst touchdown. A constant reference height selected to describe peak downburst winds will neither reflect the maximum wind speeds nor the relationship of wind speed with height for all downburst scenarios. This is in contrast to the approach taken for synoptic winds, as the widely-accepted ABL profile facilitates the use of a reference mean or gust wind speed at a height of 10m in prescribed terrain (typically open) to fully describe the magnitude and statistics of the wind load. Thus, direct comparison between a downburst wind speed and ABL wind speed at identical heights cannot provide a meaningful description of the overall differences that may exist in wind loading on a structure. A parametric investigation of the effect of downburst parameters D_{jet} and V_{jet} on the structural response of the tower is therefore carried out in the following section and compared to those obtained for a traditional ABL wind profile.

The simulated downburst wind fields (Hangan *et al*. 2003) over the height of the tower are used to evaluate the downburst wind loading. Upon analyzing the entire set of simulated wind fields, it was found that the strongest horizontal wind speed (for the range of parameters considered over the height of the tower) occurs at a distance from touchdown of r/D_{jet} = 1.3 at simulation time step t_s = 31; while other parameters are adjusted, this time step is used for all further parametric downburst scenario comparisons. Based on this position and time, the effect of D_{jet} on the horizontal wind profile normalized with respect to V_{jet} is shown in Fig. 6(a). It is shown that as D_{jet} increases, the curvature in the wind speed profile increases, tending towards a distribution resembling more of an ABL-type wind speed profile. The effects of r/D_{jet} on V_{hor}/V_{jet} for D_{jet} = 500 m are shown in Fig. 6(b), where it is shown that while the magnitude of the wind speed is greatly affected, there is not as much variation in the shape of the profile.

The numerical downburst simulation can also be used to compile a time history of horizontal wind speed at any height within the bounds of the simulation. The time histories of the horizontal wind speed at various heights are plotted in Fig. 7 for a downburst defined by r/D_{jet} = 1.3, D_{jet} = 500 m and V_{jet} = 70 m/s. The abscissa represents the time scale t at full-scale, which is calculated

based on the values of t_s, V_{jet} and D_{jet} (Hangan *et al*. 2003); each time step (i.e., increment of t_s) for this set of parameters corresponds approximately to an increment of 3.5 s, with $t_s = 0$ representing the downburst touchdown. It is shown that the peak horizontal wind speed at each of the heights occurs at t approximately equal to 109 s. Fig. 7 indicates that the downburst outflow maintains a constant speed following passage of the gust front; this is due to the assumption of steady outflow in the numerical simulation, which is a limitation of the downburst simulation and does not affect the estimation of peak responses. The wind speeds generated from the numerical downburst simulation are representative of mean peak wind speed, and accordingly gust effects are not considered in this analysis.

3.2 Applied horizontal force due to downburst

It is considered that, by assigning values of 1.0 to G_t and G_c, Eqs. (1) and (2) are applicable for calculating the downburst wind forces on the tower, although no advice on the treatment of wind loads resulting from HIW events is provided in CSA-2010. This approach is consistent with that suggested by ASCE-74 for extreme wind loading. The wind load at each node in the structural model is calculated based on the horizontal component of the downburst wind profile, and are applied to the tower model in a similar fashion to the ABL and rectangular wind loads described earlier. The wind load on the conductors and ground wire (one-half span on each side of the tower) are calculated according to Eq. (2) with G_c and G_L equal to 1.0, and the resulting forces are applied directly to the tower. Note that in this calculation, the attack angle of the wind changes along the conductors and ground wire. The variation in the downburst wind speed along the length of the wires is included in the analysis, although the effects of this for the combination of downburst parameters and wind directions investigated here is quite small.

Based on the above consideration and by adopting the simulated downburst wind speed profile, the time history of the total applied horizontal force in the longitudinal direction due to the downburst is evaluated as the sum of the applied downburst wind loads over the height of the tower.

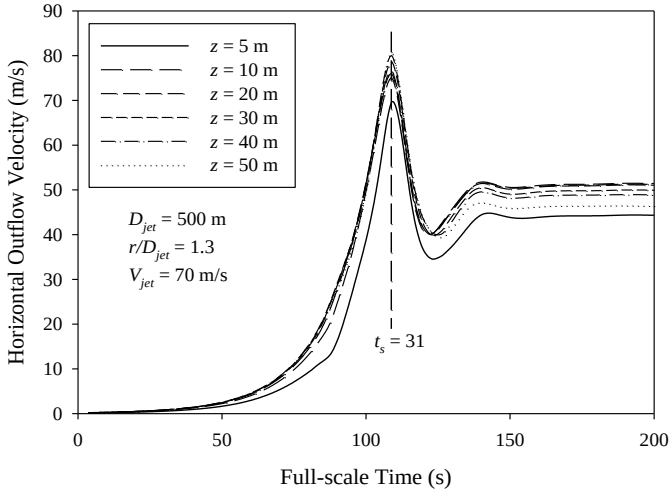

Fig. 7 Horizontal outflow velocity time history at various heights in a downburst outflow

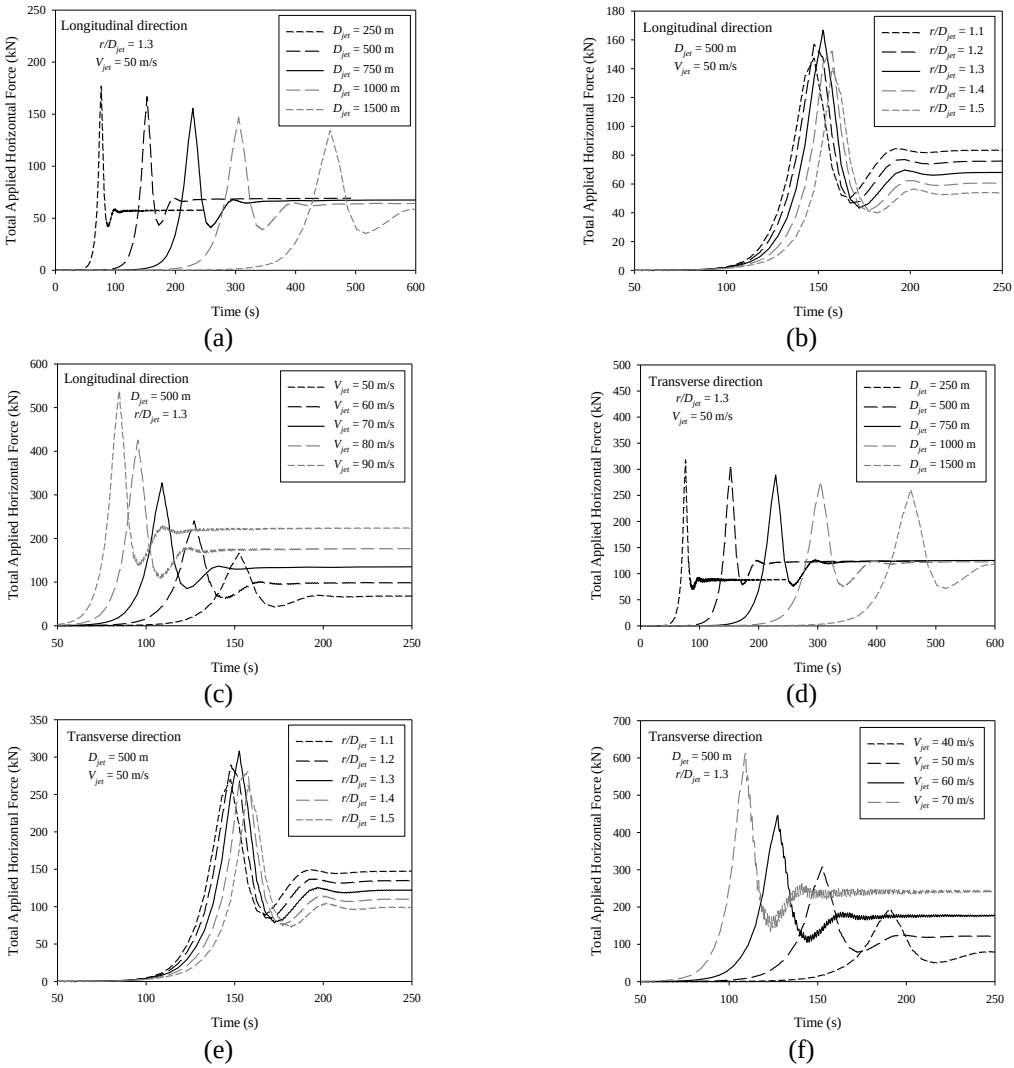

Fig. 8 Time history of the total applied horizontal force due to downburst passage varying with (a) effect of D_{jet} in the longitudinal direction,(b) effect of r/D_{jet} in the longitudinal direction, (c) effect of V_{jet} in the longitudinal direction, (d) effect of D_{jet} in the transverse direction, (e) effect of r/D_{jet} in the transverse direction and (f) effect of V_{jet} in the transverse direction

The total applied horizontal force in the longitudinal direction is shown in Fig. 8 for varying downburst parameters (i.e., D_{jet}, V_{jet}, and r/D_{jet}). The total horizontal applied force equals the base shear of the tower if the inertia force is negligible. It is shown in Fig. 8(a) that for D_{jet} ranging from 250 m to 1500 m (commonly used to characterize microburst events), the peak of the total applied horizontal force experienced by the tower during a downburst passage decreases with increasing D_{jet}. This is due to the change in the wind speed profile over the height of the tower. The variation of the total applied horizontal force for varying r/D_{jet} is shown in Fig. 8(b), indicating that the peak

load is observed for r/D_{jet} = 1.3; this is consistent with the examination of the wind speed profiles discussed for Fig. 6(a). It is therefore expected that the tower is likely to experience the greatest load effect for such a downburst scenario. The relation between the time history of the total applied horizontal force and V_{jet} is shown in Fig. 8(c), which illustrates that the peak force varies directly with V_{jet}.

Similar plots of the total applied horizontal force in the transverse direction are shown in Figs. 8(d)-8(f). For the calculation of the total applied horizontal forces, the wind loads on different portions of the wires were weighted by projected area and superimposed to generate a time history of loading on the entire wire, and were applied at the wire-tower connections. The trends shown in Figs. 8(d)-8(f) are consistent with those shown in Figs. 8(a)-8(c), although the magnitude of loading for the transverse direction is much greater due to the contributions of the conductors and ground wire.

4. Capacity curves for downburst wind loading

4.1 Capacity curves from transient and NSP analyses

A nonlinear dynamic structural analysis of the tower was first carried out considering a transient downburst passage for a downburst scenario defined by parameters D_{jet} = 500 m and r/D_{jet} = 1.3. These parameters were selected as to reflect what is believed to be a common downburst size, along with the position r/D_{jet} at which the outflow exerts the most wind load on the structure (see Fig. 8). Downburst wind speeds were simulated for a range of V_{jet} and the tower was loaded in the longitudinal and transverse directions. The obtained time history of the response in each direction was used to construct the force-deformation curves shown in Fig. 9, where the ordinate represents the total applied horizontal force (wind load) and the abscissa denotes the displacement at the tip of the tower. The figures show the linear behaviour in the elastic range, the incipient yield, and the post-yield behaviour. The response during unloading is shown following the downburst gust front, provided the tower did not fail. The jaggedness on the unloading branch is due to both the vibration of the tower and oscillation of the applied wind force. The fact that the unloading does not result in the total applied force being equal to zero is because of the sustained wind load following the passage of the downburst gust front, a consequence of the downburst model (as shown in Fig. 7). Fig. 9 shows that for some of the selected V_{jet}, the downburst passage did not initiate collapse, but was strong enough to result in a significant amount of permanent deflection. For the downburst parameters illustrated in Fig. 9, it was found that yield occurs for a V_{jet} of approximately 86 m/s and 61 m/s in the longitudinal and transverse directions, respectively, and that collapse occurred for a V_{jet} of approximately 100 m/s and 75 m/s in the longitudinal and transverse directions, respectively.

Rather than carrying out the transient analysis, which requires the knowledge of the time-varying wind speed profile, it is advantageous to carry out the NSP analysis for a single fixed wind profile if the obtained capacity curve for the latter approximates the force-deformation curve of the former. For such a purpose, the wind profile corresponding to the peak total applied horizontal force was considered, and the obtained capacity curves are compared for various downburst parameters in Fig. 9. The last point on the curves represents the analysis result obtained before non-convergence was observed in the NSP analysis. Comparison of the results shows that the use of the NSP analysis with the selected wind speed profile to evaluate the capacity curve

provides a good approximation for each direction of loading. Based on the comparison in Fig. 9, it was deemed acceptable to proceed using the NSP method to carry out a parametric investigation of downburst parameters and their influence on the capacity curve of the tower.

4.2 Sensitivity of the capacity curve to downburst parameters

Capacity curves, such as those shown in Fig. 9, are a convenient way of comparing the effects of various downburst outflow scenarios on the tower. Wind speeds are traditionally referenced to a height of 10 m, which is an appropriate method when the mean wind profile is constant throughout the duration of an event. However, as was shown in Fig. 6, the wind profile and duration in a downburst depends on both the size of the event, D_{jet}, and the distance between the structure and the downburst touchdown, r/D_{jet}. Thus, reference to a wind speed at a single height is insufficient to characterize its potential effect on a structure.

The same procedure used to evaluate the capacity curves for the ABL and rectangular wind profiles was used for the downburst profiles shown in Figs. 6(a) and 6(b); the resulting capacity curves for the longitudinal direction for combinations downburst parameters (D_{jet}, r/D_{jet}) were evaluated and are shown in Figs. 10(a) and 10(b). The capacity curves for the ABL and rectangular wind profiles are also included in the figure for comparison. It is shown in Fig. 10(a) that the tower experiences yield at similar values of deflection for each D_{jet} examined. However, the amount of deformation which the tower undergoes in the post-yield range is much more dependent on the loading profile. As D_{jet} increases, the loading profile increases in curvature over the lower half of the tower (recall Fig. 6(a)). That is, outflow profiles characterized by smaller downbursts tend to load the tower in a more uniform fashion at this distance from downburst touchdown. The low amount of post-yield deformation observed in Fig. 10(a) for D_{jet} = 250 m is due to the reduction in wind speed in the upper portion of the tower, as illustrated in Fig. 6(a). Similar comparisons are made between the capacity curves in Fig. 10(b) and the downburst outflow profiles in Fig. 6(b), although the loading profiles shown for different r/D_{jet} do not vary as much in shape as those for D_{jet}. It is shown that for the range of downburst scenarios considered, with the exception of D_{jet} = 1500 m, that the downburst capacity curves in the longitudinal direction are enveloped by those estimated using the ABL and rectangular wind profiles. Generally, the results shown in Figs. 10(a) and 10(b) indicate that as the wind loading profile becomes increasingly uniform in shape, the yield capacity of the tower increases although the post-yield deformation decreases significantly. This implies that although the maximum capacity of the tower is relatively consistent (within 4% among all the considered downburst scenarios), the post-yield behaviour of the tower is sensitive to wind load distribution.

Using the same combinations of downburst parameters as for Figs. 10(a) and 10(b), the estimation of the capacity curves in the transverse direction was carried out. The obtained curves are shown in Figs. 10(c) and 10(d), compared to those for the ABL and rectangular wind profiles. Much like the longitudinal direction, the tower experiences yield at similar values of displacement in the transverse direction for each D_{jet} examined (see Fig. 10(c)), with the case of D_{jet} = 250 m standing out due to the low wind speed at wire height (recall Fig. 6(a)). The deflection at maximum capacity for the transverse direction is much less dependent on the shape of the wind load distribution than for the longitudinal direction, and this is again due to the large loading contribution from the wires. That is, due to the loading contribution from the wires, the transverse direction is characterized by large loads in the upper portion of the tower regardless of profile.

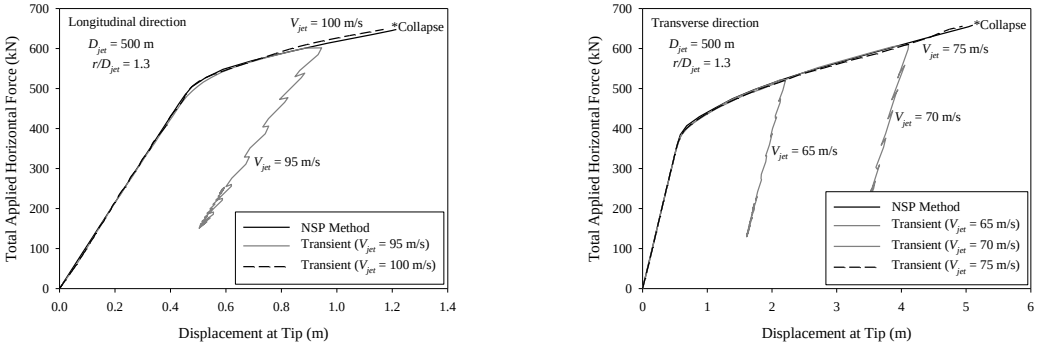

Fig. 9 Force-deformation curves for transient downburst passage with varying V_{jet} and results from NSP method for (a) longitudinal direction and (b) transverse direction

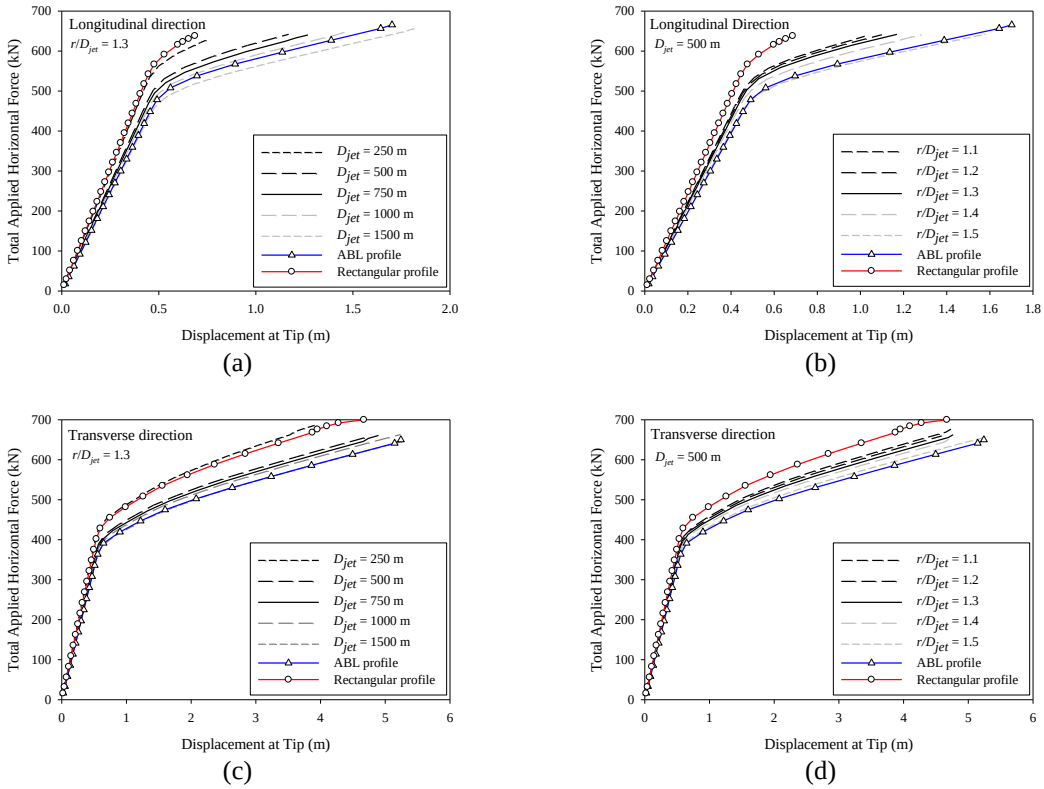

Fig. 10 Capacity curve showing the (a) effect of D_{jet} in the longitudinal direction, (b) effect of r/D_{jet} in the longitudinal direction, (c) effect of D_{jet} in the transverse direction, (d) effect of r/D_{jet} in the transverse direction

This load distribution results in a greater amount of deformation in the post-yield range observed in Figs. 10(c) and 10(d). It is shown, for the range of downburst scenarios considered, that the downburst capacity curves in the transverse direction are enveloped by those estimated using the ABL and rectangular wind profiles.

To better appreciate the characteristics of tower capacity at the incipient yield and collapse, their values are estimated based on the capacity curves shown in Fig. 10. The calculated capacities were used to estimate the ratios of the yield and maximum capacities under downburst loading to the rectangular and ABL wind profiles which are shown in Table 5. The values suggest that the ABL wind profile provides a conservative (or very close) estimate of the yield capacity of the tower under downburst loading, while the maximum capacity in the longitudinal and transverse directions are slightly underestimated (within 5%) and overestimated (within 6%), respectively. The rectangular wind profile provides good estimates of the yield and maximum capacity under smaller downburst events, as well as the maximum capacity in the longitudinal direction for each downburst scenario. A conservative estimate of the yield capacity under larger downburst events, and capacity in the transverse direction in general, is made using the ABL wind profile.

Table 5 Ratios of yield and maximum capacities (kN) under downburst wind loading to those associated ABL and rectangular wind profiles

r/D_{jet} = 1.3								
	Capacity Ratio: Downburst to ABL				Capacity Ratio: Downburst to Rectangular			
	Longitudinal		Transverse		Longitudinal		Transverse	
D_{jet} (m)	Yield	Maximum	Yield	Maximum	Yield	Maximum	Yield	Maximum
250	1.05	0.95	1.12	1.06	0.96	0.99	1.02	0.98
500	0.97	0.96	1.05	1.02	0.90	1.01	0.96	0.95
750	1.02	0.96	1.05	1.02	0.94	1.00	0.95	0.94
1000	1.00	0.97	1.02	1.02	0.92	1.01	0.93	0.95
1500	0.98	0.99	1.00	0.99	0.90	1.03	0.90	0.92
D_{jet} = 500 m								
	Longitudinal		Transverse		Longitudinal		Transverse	
r/D_{jet}	Yield	Maximum	Yield	Maximum	Yield	Maximum	Yield	Maximum
1.1	1.02	0.96	1.08	1.04	0.94	1.00	0.98	0.97
1.2	1.00	0.96	1.04	1.02	0.92	1.00	0.94	0.94
1.4	1.03	0.96	1.04	1.00	0.94	1.00	0.94	0.93
1.5	0.99	0.98	1.01	1.01	0.91	1.02	0.92	0.94

5. Conclusions

Analyses have been carried out to estimate the nonlinear inelastic response of a self-supported lattice transmission tower under different types of wind loading. For the analysis, the tower was represented by a 3-D numerical model which considers both material and geometric nonlinearity. The NSP method, which is most commonly used for earthquake loading, was used to assess the tower capacity under ABL, rectangular and downburst wind load profiles. Also, the transient analysis linear and nonlinear dynamic analysis was carried out for modeled downburst wind load. The analysis results were used to develop the capacity curve of the tower, which is represented using the base shear versus the displacement at the tip of the tower. The following conclusions are drawn from the analysis:

1. The capacities of the tower at incipient yield and at incipient collapse depend on the wind loading profile. Generally, the capacities to sustain wind load for the ABL wind profile are lower than those for the rectangular wind profile. The uncertainty in the capacity estimation due to material properties and geometric variables is not very significant; the coefficient of variation of the capacity was found to be less than 10%, which is significantly smaller than that associated with the total wind load effect.

2. The wind load on the conductors and ground wire significantly affect the capacity curves in the transverse direction (as compared to the longitudinal direction). The critical wind speed for the considered tower is associated with the transverse direction.

3. The capacity curves obtained for the ABL and rectangular wind profiles can be used as approximate lower and upper bounds for the capacity curve resulting from important downburst wind profiles. The use of capacity curves avoids the difficulty associated with defining a representative reference height for wind speeds in downburst conditions.

4. Downbursts which are smaller in size result in the tower experiencing yield at a higher base shear, as well as less deformation with increasing wind speed. Downbursts which are greater in size initiate yield at a lower horizontal wind load, but allow for more deformation in the post-yield range leading up to collapse. The characteristics (yield and maximum capacity) of the capacity curve for the ABL wind load distribution resembles that for a downburst characterized by a D_{jet} between 1000 m and 1500 m. As the size of the downburst increases, the capacity curve becomes steeper in both the elastic and inelastic range.

5. Based on the above observations, it is recommended that the capacity curve estimated under the rectangular wind profile can be used as a proxy for the capacity curve associated with small downburst events, and that the capacity curve estimated under the ABL wind profile can be used as a proxy for the capacity curve if the downburst size is large. The consideration of these conditions in practice simplifies the performance assessment of towers under downburst wind loading, as well as provides advice on the capacity required for towers to resist downburst winds at the design stage.

Acknowledgements

The downburst wind fields were made available by Dr. H.M. Hangan of the WindEEE Research Institute at the University of Western Ontario. The financial support from the National Sciences and Engineering Research Council of Canada (NSERC) is gratefully acknowledged. The contributions of Mr. S. Yang are also gratefully acknowledged.

References

American Society of Civil Engineers (ASCE) (2010), *Guidelines for Electrical Transmission Line Structural Loading (3rd edition), ASCE Manuals and Reports on Engineering Practice No. 74*, Reston, VA, USA.

ANSYS® (2007), ANSYS Multiphysics, Release 9.0. ANSYS Inc., Canonsburg, PA.

Banik, S.S., Hong, H.P. and Kopp, G.A. (2008), "Assessment of tornado hazard for spatially distributed systems in southern Ontario", *J. Wind Eng. Ind. Aerod.*, **96**(8-9), 1376-1389.

Banik, S.S., Hong, H.P. and Kopp, G.A. (2010), "Assessment of capacity curves for transmission line towers under wind loading", *Wind Struct.*, **13**(1), 1-20.

Bartlett, F.M., Hong, H.P. and Zhou, W. (2003), "Load factor calibration for the proposed 2005 edition of the National Building Code of Canada: Statistics of loads and effects", *Can. J. Civ. Eng.*, **30**(2), 429-439.

Canadian Standards Association (CSA) (2010), *Design criteria of overhead transmission lines, CAN/CSA-C22.3 No. 60826-10*, CSA, Toronto, Canada.

Darwish, M.M. and El Damatty, A.A. (2011), "Behaviour of self supported transmission line towers under stationary downburst loading", *Wind Struct.*, **14**(5), 481-498.

Davenport, A.G. (1979). "Gust response factors for transmission lines", *Proceedings of the 5th International Conference on Wind Engineering*, Fort Collins, CO, USA.

Durst, C.S. (1960), "Wind speeds over short periods of time", *Met. Mag.* **89**, 181-186.

Ellingwood, B.R., Galambos, T.V., MacGregor, J.G. and Cornell, C.A. (1980). *Development of a probability based load criterion for American National Standard A58*, National Bureau of Standards, Washington D.C., USA.

Fujita, T.T. (1976), *Spearhead Echo and Downburst near the Approach end of a John F. Kennedy Airport Runway, New York City, SMRP Research Paper No. 137*, University of Chicago.

Fujita, T.T. (1985), *The Downburst: Microburst and Macroburst, SMRP Research Paper No. 210*, University of Chicago.

Hangan, H., Roberts, D., Xu, Z. and Kim, J.D. (2003), "Downburst simulations. Experimental and numerical challenges", *Proceedings of the 11th International Conference on Wind Engineering*, Lubbock, TX, USA.

Hangan, H., Savory, E., El Damatty, A., Galsworthy, J. and Miller, C. (2008), "Modeling and prediction of failure of transmission lines due to high intensity winds", *Proceedings of the 2008 Structures Congress (ASCE)*, Vancouver, BC, Canada.

Haukaas, T. and Der Kiureghian, A. (2006), "Strategies for finding the design point in non-linear finite element reliability analysis", *Probabilist. Eng. Mech.*, **21**(2), 133-147.

He, W.X. and Hong, H.P. (2012), "Probabilistic characterization of roof panel uplift capacity under wind loading", *Can. J. Civ. Eng.*, **39**(12), 1285-1296.

Holmes, J.D. and Oliver, S.E. (2000), "An empirical model of a downburst", *Eng. Struct.*, **22**(9), 1167-1172.

Holmes, J.D., Hangan, H.M., Schroeder, J.L., Letchford, C.W. and Orwig, K.D. (2008), "A forensic study of the Lubbock-Reese downdraft of 2002", *Wind Struct.*, **11**(1), 137-152.

Hong, H.P., Mara, T.G., Morris, R., Li, S.H. and Ye, W. (2014). "Basis for recommending an update of wind velocity pressures in Canadian design codes." *Can. J. Civ. Eng*., 41(3), 206-221.

Kim. J. and Hangan, H. (2007), "Numerical simulation of impinging jets with application to downbursts", *J. Wind Eng. Ind. Aerod.*,, **95**(4), 279-298.

Krawinkler, H. and Seneviratna, G.D.P.K. (1998), "Pros and cons of a pushover analysis of seismic performance evaluation", *Eng. Struct.*, **20**(4-6), 452-464.

Lee, P.S. and McClure, G. (2007), "Elastoplastic large deformation analysis of a lattice steel tower structure and comparison with full-scale tests", *J. Constr. Steel Res.*, **63**(5), 709-717.

Lee, K.H. and Rosowsky, D.V. (2006), "Fragility curves for woodframe structures subjected to lateral wind load", *Wind. Struct.*, **9**(3), 217-230.

Lin, W.E., Savory, E., McIntyre, R.P., Vandelaar, C.S. and King, J.P.C. (2012), "The response of an overhead electrical power transmission line to two types of wind forcing", *J. Wind Eng. Ind. Aerod.*, **100**(1), 58-69.

Lombardo, F.T. (2009), *Analysis and interpretation of thunderstorm wind flow and its effect on a bluff body*. Ph.D. Dissertation, Texas Tech University.

Lombardo, F.T., Smith, D.A., Schroeder, J.L. and Mehta, K.C. (2014), "Thunderstorm characteristics of importance to wind engineering", *J. Wind Eng. Ind. Aerod*., **125**, 121-132.
Mara, T.G., Galsworthy, J.K. and Savory, E. (2010), "Assessment of vertical wind loads on lattice framework with application to thunderstorm winds", *Wind Struct.*, **13(**4), 413-431.
Mara, T.G. and Hong, H.P. (2013), "Effect of wind direction on the response and capacity surface of a transmission tower", *Eng. Struct*., **57**, 493-501.
McCarthy, P. and Melsness, M. (1996), *Severe Weather Elements Associated with September 5, 1996 Hydro Tower Failures Near Grosse Isle, Manitoba, Canada*, Environment Canada, Winnipeg, Canada.
Orwig, K.D. and Schroeder, J.L. (2007), "Near-surface wind characteristics of extreme thunderstorm outflows", *J. Wind Eng. Ind. Aerod*.,, **95(**7), 565-584.
Savory, E., Parke, G.A.R., Zeinoddini, M., Toy, N. and Disney, P. (2001), "Modelling of tornado and microburst-induced wind loading and failure of a lattice transmission tower", *Eng. Struct.*, **23(**4), 365-375.
Shehata, A.Y., El Damatty, A.A. and Savory, E. (2005), "Finite element modeling of transmission line under downburst wind loading", *Finit. Elem. Anal. Des*., **42(**1), 71-89.
Shehata, A.Y. and El Damatty, A.A. (2008), "Failure analysis of a transmission tower during a microburst", *Wind Struct*., **11**(3), 193-208.
Wood, G.S., Kwok, K.C.S., Motteram, N.A. and Fletcher, D.F. (2001), "Physical and numerical modelling of thunderstorm downbursts", *J. Wind Eng. Ind. Aerod*., **89**(6), 535-552.

JH